

Sensorless Small-Scale Variable Speed Wind Energy Conversion System Incorporating DTC-SVM of Direct-Drive PMSG with RLC Filter

Pieter Bouwer and Maarten J Kamper, *Senior Member, IEEE*
Department of Electrical and Electronic Engineering
Stellenbosch University
Stellenbosch, South Africa
kamper@sun.ac.za

Abstract—In this study a complete mechanical sensorless small-scale, fixed-pitch variable speed, wind energy conversion system is implemented that uses a permanent magnet synchronous generator with RLC filter, that is controlled using direct torque control with space vector modulation. Mathematical models of the system are derived and presented. The system is simulated in VHDL-AMS using Mentor Graphics SystemVision as well as MATLAB Simulink and results are presented. A gain scheduling algorithm is designed for stable operation across the entire operating range. The system is then implemented on a laboratory setup and results are presented.

I. INTRODUCTION

The trend in the field of wind energy is towards variable speed systems incorporating direct-drive permanent magnet synchronous generators (PMSGs) with full scale power electronic converters (PECs), mainly due to improved energy capture, reduced mechanical stresses, higher efficiency and reliability [1]. According to [1] a variable speed system can capture up to 15% more energy than a comparable single fixed speed system.

An LC output filter is especially necessary if long cables are used from the converter to the generator [2], which is mostly the case in a wind energy conversion system (WECS). The filter also provides motor friendly voltages and higher power quality [3] which extends the lifetime of the generators as well as reduces maintenance issues.

Transient or sustained resonances may occur with the presence of an LC filter, which may cause serious instability. It is therefore necessary to damp these resonances either actively or passively. In this study damping resistances are placed in series with the LC filter capacitors – it is therefore more technically correct to refer to the filter as an RLC filter, as the resistance component now contributes significantly to the dynamic properties of the filter.

The application of direct torque control (DTC) to WECSs is a relatively new concept. In [4] it is concluded that due to its insensitivity to physical parameters, inherent sensorless operation and ease in implementing variable speed strategies, DTC is more suited in WECSs than the classic FOC. However, the implementation in [4] does not implement an LC filter. In [5] the authors apply DTC with space vector modulation

(DTC-SVM) to wind energy, but their scheme is not direct-driven, sensorless or with an LC filter. In [6] classic DTC for maximum power point tracking (MPPT) control of a PMSG is used, but the system is neither sensorless nor with an LC filter.

In this paper a complete mechanical sensorless WECS, incorporating DTC-SVM of a PMSG with an RLC filter is implemented. Modeling for parallel structure DTC-SVM done in [7] is extended to include the effects of the RLC filter.

It must be emphasized that this is a small-scale system¹, which forms part of the motivation for a fixed pitch system. It is also part of the objectives of this research to implement a WECS with as few as possible moving parts, hence the direct-driven approach.

The sensorless DTC-SVM implemented on the PMSG including LC filter is simulated in VHDL-AMS using SystemVision by Mentor Graphics as well as MATLAB Simulink. A gain scheduling (GS) algorithm including the controllers is implemented practically on a laboratory test setup.

This study is mainly concerned with the generator side of the WECS, and grid connection issues and transients are not dealt with in this paper.

II. SYSTEM OVERVIEW AND DESCRIPTION

An overview of the system is presented in Fig. 1. The GS algorithm selects between two controllers, $D_s(s)$ and $f(\hat{\omega}_r)$, which are fixed speed control and MPPT control respectively, according to the system's estimated variables. The *Estimation* block represents all the estimation components of the system that are required for the system to achieve sensorless operation. The controllers generate a torque command m_f^* as an input to the DTC-SVM component, which in turn generates the duty cycle for the switching of the IGBT's. The generator currents \vec{i}_s and voltages \vec{v}_s are the only measured variables, from which all other system variables are estimated.

III. SYSTEM MODELLING

The mechanical equations that describe the dynamics of the generator rotor and turbine are

¹There is no universal definition as of yet, but some sources agree on a power rating of less than 100 kW.

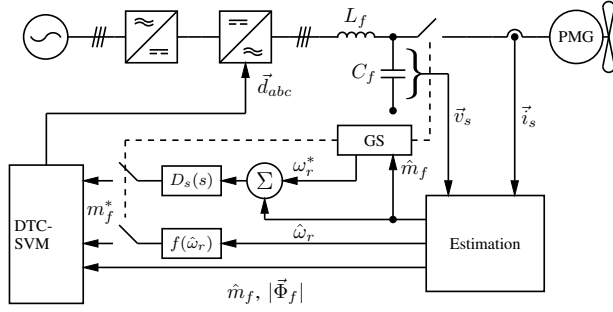


Fig. 1: Representation of the system.

$$J \frac{d\omega_m}{dt} = m_e - m_L, \quad (1a)$$

$$\omega_r = N_p \omega_m, \quad (1b)$$

$$\omega_r = \frac{d\theta_r}{dt}. \quad (1c)$$

where J represents the combined inertia of the rotor and turbine, ω_m and ω_r the mechanical and electrical rotational speeds of the rotor, respectively, m_L and m_e the turbine torque and electromagnetic torque, respectively, and N_p the number of pole pairs of the PMSG.

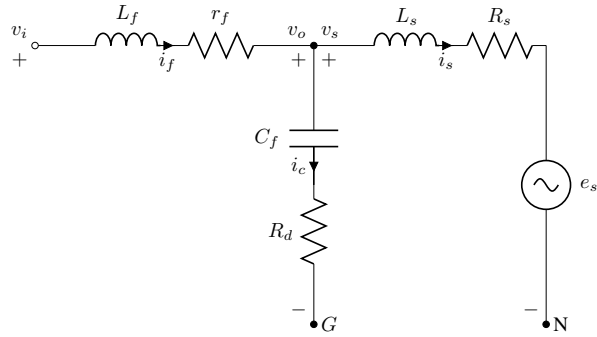


Fig. 2: Single line circuit diagram representation of the three phase system.

The single line circuit diagram of the RLC filter plus PMSG is presented in Fig. 2. Using simple nodal circuit analysis, the system can be described by

$$\vec{v}_i = r_f \vec{i}_f + L_f \frac{d\vec{i}_f}{dt} + \vec{v}_o, \quad (2a)$$

$$\vec{v}_s = R_s \vec{i}_s + L_s \frac{d\vec{i}_s}{dt} + \vec{e}_s = R_s \vec{i}_s + \frac{d\vec{\Phi}_s}{dt}, \quad (2b)$$

$$\vec{\Phi}_s = L_s \vec{i}_s + \Phi_m \begin{bmatrix} \cos(\theta_r) \\ \cos(\theta_r - \frac{2\pi}{3}) \\ \cos(\theta_r + \frac{2\pi}{3}) \end{bmatrix}, \quad (2c)$$

$$\vec{v}_o = \frac{1}{C_f} \int \vec{i}_c dt + R_d \vec{i}_c. \quad (2d)$$

where $\vec{\Phi}_s$ is the stator flux linkage, Φ_m the permanent magnet flux and θ_r the rotor position of the PMSG.

The vectored (e.g. \vec{x}_s) variables in (2) represent vectors of three-phase components, a , b and c . This notation is also used to represent vectors of two dimensions in both the stationary and flux linkage synchronously rotating reference frames further on.

The expression for the stator flux linkage $\vec{\Phi}_s$ assumes that the three-phase system is positive phase sequenced.

What is important to note from the equations given in (2) is that the RLC filter output voltage is not the same as the line to neutral terminal voltage of the generator. The voltage between the generator and filter neutral points is not zero – from work done in [8] it can be shown that the equation in (3) holds true.

It is assumed that the neutral points of the inverter and that of the RLC filter are connected, even though they are not in practice. The neutral point of the the inverter output can however be arbitrarily chosen as being the same as the RLC filter², which simplifies modelling.

It can be deduced that the the stator terminal voltages of the PMSG and the line to neutral voltages of the RLC filter output are related by (3) [8]. This clearly shows coupling between the three phases and would make modelling the system by means of transfer function models quite difficult.

$$\begin{bmatrix} v_{sa} \\ v_{sb} \\ v_{sc} \end{bmatrix} = \frac{1}{3} \cdot \begin{bmatrix} 2 & -1 & -1 \\ -1 & 2 & -1 \\ -1 & -1 & 2 \end{bmatrix} \cdot \begin{bmatrix} v_{ca} \\ v_{cb} \\ v_{cc} \end{bmatrix}. \quad (3)$$

Now the voltages are transformed into the stationary reference frame($\alpha\beta$ -reference frame) by using (3), (4a) and (4b).

$$K_s = \sqrt{\frac{2}{3}} \cdot \begin{bmatrix} 1 & -\frac{1}{2} & -\frac{1}{2} \\ 0 & -\frac{\sqrt{3}}{2} & \frac{\sqrt{3}}{2} \\ \frac{1}{\sqrt{2}} & \frac{1}{\sqrt{2}} & \frac{1}{\sqrt{2}} \end{bmatrix}, \quad (4a)$$

$$K_s^{-1} = K_s^T, \quad (4b)$$

$$\begin{bmatrix} v_{s\alpha} \\ v_{s\beta} \end{bmatrix} = \frac{1}{3} \cdot K_s \cdot \begin{bmatrix} 2 & -1 & -1 \\ -1 & 2 & -1 \\ -1 & -1 & 2 \end{bmatrix} \cdot K_s^{-1} \cdot \begin{bmatrix} v_{c\alpha} \\ v_{c\beta} \end{bmatrix} \quad (4c)$$

$$= \begin{bmatrix} v_{c\alpha} \\ v_{c\beta} \end{bmatrix}. \quad (4d)$$

The output voltages of the RLC filter and the terminal voltages of the generator can now be used interchangeably. The derived equations in the $\alpha\beta$ -reference frame are given in (5).

$$\vec{v}_{i,\alpha\beta} = R_f \vec{i}_{f,\alpha\beta} + L_f \frac{d\vec{i}_{f,\alpha\beta}}{dt} + \vec{v}_{o,\alpha\beta}, \quad (5a)$$

$$\vec{v}_{o,\alpha\beta} = \frac{1}{C_f} \int \vec{i}_c dt + R_d \vec{i}_c, \quad (5b)$$

$$\vec{v}_{s,\alpha\beta} = R_s \vec{i}_{s,\alpha\beta} + \frac{d\vec{\Phi}_{s,\alpha\beta}}{dt}, \quad (5c)$$

$$\vec{\Phi}_{s,\alpha\beta} = L_s \vec{i}_{s,\alpha\beta} + \Phi_f \begin{bmatrix} \sin \theta_r \\ \cos \theta_r \end{bmatrix}, \quad (5d)$$

²This only dictates where the output is then "measured".

$$m_e = \left(\frac{3}{2}\right) N_p (\Phi_{s\alpha} i_{s\beta} - \Phi_{s\beta} i_{s\alpha}). \quad (5e)$$

To implement a parallel structure DTC-SVM algorithm, the system must be expressed in the stator flux linkage synchronously rotating reference frame (xy -reference frame). The reference frame in this regard rotates in synchronism with the stator flux linkage of the permanent magnet wind generator.

The system equations in the xy -reference frame are obtained by applying the transformation matrix in (6) to (5).

$$K_{xy} = \begin{bmatrix} \cos \gamma_s & \sin \gamma_s \\ -\sin \gamma_s & \cos \gamma_s \end{bmatrix}. \quad (6)$$

The xy -reference frame equations of the system are then

$$\vec{v}_{i,xy} = R_f \vec{i}_{f,xy} + L_f \frac{d\vec{i}_{f,xy}}{dt} + L_f \omega_\Phi \begin{bmatrix} -i_{fy} \\ i_{fx} \end{bmatrix} + \vec{v}_{o,xy}, \quad (7a)$$

$$\vec{v}_{o,xy} = R_d \vec{i}_{c,xy} + \vec{v}_{c,xy}, \quad (7b)$$

$$\vec{i}_{c,xy} = C_f \frac{d\vec{v}_{c,xy}}{dt} + C_f \omega_\Phi \begin{bmatrix} -v_{cy} \\ v_{cx} \end{bmatrix}, \quad (7c)$$

$$\vec{v}_{s,xy} = R_s \vec{i}_{s,xy} + \frac{d\vec{\Phi}_{s,xy}}{dt}, \quad (7d)$$

$$\Phi_{sx} = L_s i_{sx} + \Phi_m \cos \delta, \quad (7e)$$

$$0 = L_s i_{sy} - \Phi_m \sin \delta, \quad (7f)$$

$$m_e = \left(\frac{3}{2}\right) N_p \Phi_{sx} i_{sy}, \quad (7g)$$

$$\delta = \gamma_s - \theta_r, \quad (7h)$$

$$\omega_\Phi = \frac{d\gamma_s}{dt} = \omega_r + \frac{d\delta}{dt}. \quad (7i)$$

where ω_Φ is the filter-generator frequency, γ_s the stator flux position angle and δ the power angle of the PMSG.

The coupling between the x and y components as well as dependency on system frequency are clear and arise due to the inclusion of the RLC filter.

Due to the addition of the RLC filter the terminal voltages of the generator, and consequently the torque and flux linkage, are no longer directly controlled. It is now necessary to define the filter-generator torque m_f and filter-generator flux linkage Φ_f which will become the new controlled variables. The expressions of the new controlled parameters are given in (8) [2][9].

$$\vec{\Phi}_{f,xy} = L_f \vec{i}_{f,xy} + \vec{\Phi}_{s,xy}, \quad (8a)$$

$$m_f = \left(\frac{3}{2}\right) N_p (\Phi_{fx} i_{fy} - \Phi_{fy} i_{fx}). \quad (8b)$$

The equations in (8) have the same form in both the $\alpha\beta$ - and xy -reference frames.

IV. SENSORLESS OPERATION

Mechanical sensorless machine control generally has to do with how one obtains information on rotor position. A multitude of rotor position estimation techniques exist, but they can generally be divided into high frequency injection methods and calculation methods.

Specifics on these methods will not be dealt with in this paper, but the most important distinction to make is that high frequency injection methods are good for lower rotational speeds to standstill, while the calculation method is good for medium to high speeds.

As significant wind speeds³ are of interest in WECS, which imply higher rotor speeds, the calculation method will be sufficient in this regard.

The rotor position is easily obtained from the generator back-emf voltage from (9).

$$\begin{bmatrix} e_{s\alpha} \\ e_{s\beta} \end{bmatrix} = \omega_r \Phi_m \begin{bmatrix} \cos \theta_r \\ -\sin \theta_r \end{bmatrix}. \quad (9)$$

A simple yet very effective and accurate observer proposed in [10] is implemented in this study. It is a simple Luenberger observer observing in the $\alpha\beta$ -reference frame, identical for both α and β components. A diagram of this EEMF observer can be seen in Fig. 3.

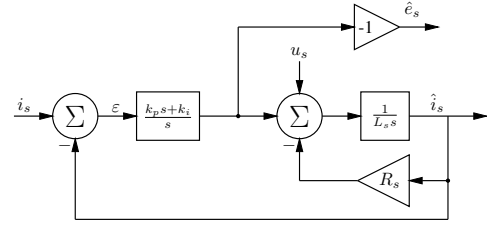


Fig. 3: Block diagram representation of the EEMF observer proposed by Yang et. al..

The hatted variables (e.g. \hat{x}_s) as in Fig. 3 and elsewhere refer to estimated variables.

Both the magnitude and angle of the stator flux linkage is needed to achieve DTC-SVM. A very common and simple estimator employing the combined voltage-current model of stator flux [11] is used in this system.

A diagram of the flux linkage observer is shown in Fig. 4, which estimates the stator flux linkage in the stationary reference frame. The magnitude and phase angle can then be easily obtained from the estimated flux linkage.

The rotor speed is obtained from the estimated rotor angle by taking the approximate digital derivative and low pass filtering. This method delivers satisfactory performance to fulfil the goals of this study, however a more robust estimation method would be desirable for practical implementation.

A model reference adaptive system (MRAS) has been used in the Simulink simulations to obtain a better estimate of the rotor speed. This technique failed in both the VHDL-AMS simulations and in practice as the MRAS output could not reach stability. It is still unclear what exactly caused the

³Wind speeds at which it is efficient to convert energy.

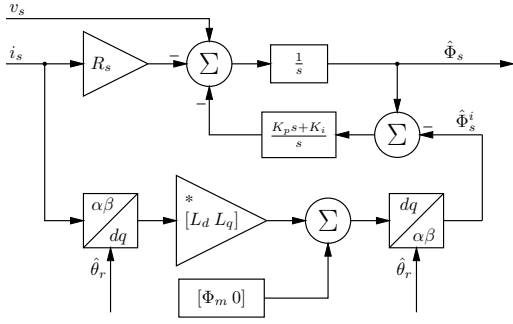


Fig. 4: Block diagram representation of the combined voltage-current model flux estimator.

instability, but it the assumption is that switching noise is to blame.

V. DIRECT TORQUE CONTROL

The main disadvantages of classic DTC have been overcome with the introduction of DTC with space vector modulation (DTC-SVM). The use of SVM ensures a constant switching frequency as well as a significantly reduced torque ripple. The modelling and controller design is also simplified, as the voltage vector switching is done by the SVM [7].

The details of either DTC or SVM will not be dealt with in this paper, as they have been so widely publicised.

A. Parallel Structure DTC-SVM

Parallel structure DTC-SVM resides in the xy -reference frame. In work done in [7] it is shown that the parallel structure yields superior performance, additional to providing simpler controller design. A diagrammatic representation is shown in Fig. 5.

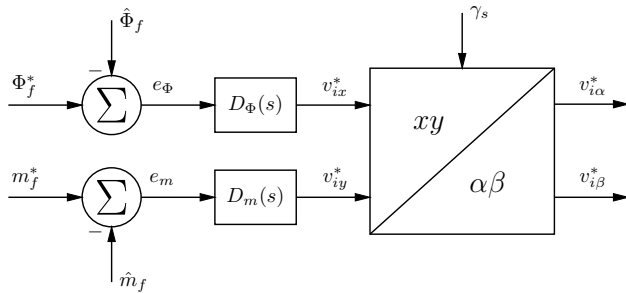


Fig. 5: Controller representation of parallel-structure DTC-SVM.

The controller transfer functions $D_\Phi(s)$ and $D_m(s)$ are PI based controllers. The flux reference is kept constant at a nominal value in this study, while the torque reference is determined by the relevant control scheme. The generated control voltages are transformed back to the stationary frame for SVM.

B. Approximate Transfer Functions

To design the controllers for both the torque and flux linkage, approximate transfer functions can be derived to which

familiar control theory can be applied. Building on work done in [7], approximate transfer functions for the system including the sinus filter with damping resistances are derived, using the system equations expressed in the xy -reference frame (7).

Simplifying assumptions that are made are that the coupling between the x and y components in (7) are ignored, the magnitude of flux linkage $|\Phi_f|$ in some cases is assumed to be constant and equal to permanent magnet flux linkage Φ_m and the filter-generator frequency ω_Φ is assumed to be equal to the generator electrical frequency ω_r . Some coefficients have also been simplified during the derivation, based on relative parameter values. The derivation is not included in the paper due to space limitations.

The approximate transfer functions are then obtained as

$$G_m(s) = \frac{V_{iy}(s)}{M_f(s)} = \frac{A_m (\beta_3 s^3 + \beta_2 s^2 + \beta_1 s)}{\alpha_4 s^4 + \alpha_3 s^3 + \alpha_2 s^2 + \alpha_1 s + \alpha_0}, \quad (10a)$$

$$G_\Phi(s) = \frac{V_{ix}(s)}{\Phi_f(s)} = \frac{A_\Phi (b_2 s^2 + b_1 s + b_0)}{a_3 s^3 + a_2 s^2 + a_1 s + a_0}. \quad (10b)$$

The coefficients are presented in Table I. The coefficients consist of the system parameters, of which values for this specific study are given in Table III.

TABLE I: Coefficients of derived transfer function models of torque and flux linkage plants.

Flux Linkage Plant		Torque Plant	
Coefficient	Expression	Coefficient	Expression
A_Φ	$\frac{1}{L_f C_f}$	A_m	$\frac{3\Phi_m N_p}{2L_s}$
b_2	$L_f C_f$	β_3	$L_s C_f$
b_1	$R_d C_f$	β_2	$R_d C_f$
b_0	1	β_1	1
a_3	1	α_4	$L_f C_f$
a_2	$\frac{R_d}{L_f}$	α_3	$(R_d + r_f) C_f$
a_1	$\frac{1}{L_f C_f}$	α_2	1
a_0	$\frac{r_f}{L_f C_f L_s}$	α_1	$\frac{r_f}{L_s}$
		α_0	$\frac{N_p \Phi_m}{J}$

Due to their complexity, it would be difficult to use these transfer functions in the design of controllers, but they will allow us to observe the significant effect the higher order poles have on the dynamic performance of the system. The full effects of the damping resistances can also be observed.

The derived approximate transfer functions in (10) can be further simplified as

$$G_m(s) = \frac{A_m s}{s^2 + \alpha_1 \cdot s + \alpha_0}, \quad (11a)$$

$$G_{\Phi}(s) = \frac{1}{s + \frac{a_0}{a_1}}. \quad (11b)$$

The closed loop transfer functions, including the PI controllers, are then obtained as

$$G_{m,CL} = \frac{A_m (k_{p,m}s + k_{i,m})}{s^2 + (\alpha_1 + A_m k_{p,m})s + \alpha_0 + A_m k_{i,m}}, \quad (12a)$$

$$G_{\Phi,CL} = \frac{k_{p,\Phi}s + k_{i,\Phi}}{s^2 + \left(\frac{a_0}{a_1} + k_{p,\Phi}\right)s + k_{i,\Phi}}. \quad (12b)$$

where k_i and k_p denote integral and proportional gains of the PI controllers, respectively.

Control theory can now be easily applied to the closed loop transfer functions to obtain the desired transient dynamic response. The maximum gains are further limited by the higher order poles contained in the more accurate transfer functions and any design should be verified for stability.

VI. TORQUE REFERENCE GENERATION

In the complete system the torque reference m_f^* for the DTC-SVM is generated by either the constant speed controller $D_s(s)$ or the variable speed MPPT controller $f(\hat{\omega}_r)$, depending on the current state of the GS algorithm.

A. Constant Speed Controller

Although the main objective of this WECS is variable speed operation, there is need of speed control in certain operating regions as well as during transitions between these regions. This is essential for proper operation of the system. The bandwidth of the speed controller does not need to be wide, due to the large inertia inherent in any WECS, as well as naturally slow changing wind conditions.

B. Variable Speed MPPT Controller

This is the most important control operation of the system, as this defines the main control objective. For this paper a very simple MPPT algorithm, that simply calculates the optimal instantaneous torque command based on a function of the current rotor speed, is implemented. The torque command generation algorithm is

$$m_f^* = f(\hat{\omega}_r) = k_{f1}\hat{\omega}_r^2 + k_{f2}\hat{\omega}_r. \quad (13)$$

A polynomial is fitted to blade curve data to obtain coefficients k_{f1} and k_{f2} . It should be stressed that this MPPT method is sensitive to parameter variation of the wind turbine.

VII. GAIN SCHEDULING

Gain scheduling (GS), simply defined, is the dividing up of a system's entire operating range into smaller operating regions. This can be seen as a type of linearisation of a non-linear system. A more detailed exposition of GS theory is given in [12]. For this system a simple GS algorithm is developed to facilitate the operation of the system. A state diagram representation of the GS algorithm is given in Fig. 6.

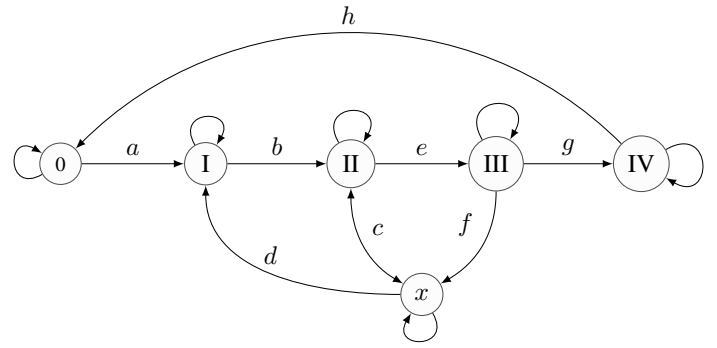


Fig. 6: State diagram of gain scheduling algorithm.

A table summarising the states and their descriptions is given in Table II. The letters a through f represent transitions between the states that occur when a certain set of conditions are satisfied. The arrows on the transitions show the direction in which a transition can occur.

TABLE II: Description of the states of the GS algorithm.

0	<i>Pre-states:</i> The generator is desynchronised and the system waits for the rotor speed (representing the wind speed) to be below a certain threshold, and then transitions to the next state once this threshold is breached.
I	<i>Pre-cut-in:</i> The system waits for the rotor speed to exceed a threshold before transitioning to the next state. <i>Cut-in:</i> After synchronising with the generator, the generator speed is controlled at cut-in speed until the wind speed breaches a determined threshold, which is determined by monitoring electromagnetic torque generation. Transitioning can either be towards state x : <i>Cut-out</i> or state III: <i>MPPT</i>
II	<i>MPPT:</i> The generator torque is controlled as a function of rotor speed to achieve MPPT. This is the variable speed state of the WECS where it is desirable to spend most of the time.
III	<i>Max Speed:</i> When the maximum speed constraint of the system is reached, the generator speed is controlled at this maximum speed. Transitioning can either be back towards state III or to state 0 (desynchronisation), depending on wind conditions.
IV	<i>Cut-out:</i> The generator is controlled at a certain cut-out speed after certain conditions have been met in states II and III, and waits either for the wind speed to decrease sufficiently for desynchronisation, or to increase sufficiently to return to state II.
x	

VIII. SIMULATION METHODOLOGY

The main simulation framework for this research is chosen as VHDL-AMS. The language provides very intuitive and modular structural elements which make the description of hardware systems very natural. Another advantage is the seamless combination of digital and analogue signals in the simulation. This allows for effective integrated physical systems which are controlled by digital control systems.

As MATLAB Simulink has become an industry standard in most engineering fields, it has been used alongside VHDL-AMS to model the system presented in this paper. As VHDL-AMS has not been widely adopted in industry, this serves as a

good comparison to test the effectiveness thereof as compared to an industry standard. The motivation for developing the Simulink model is therefore mostly for verification purposes.

An interesting thing to note is the major difference between the two methods of simulation. Simulink uses a graphical interface to represent system models, while the VHDL-AMS approach is an entirely coded method⁴.

A. Simulink

A diagram of the system model as modelled in Simulink is shown in Fig. 7. The time-domain equations in the $\alpha\beta$ -reference frame (5) describing the system have been converted to the Laplace domain to obtain transfer function models. The final implementation, however, is a mixture of Laplace- and time-domain parts.

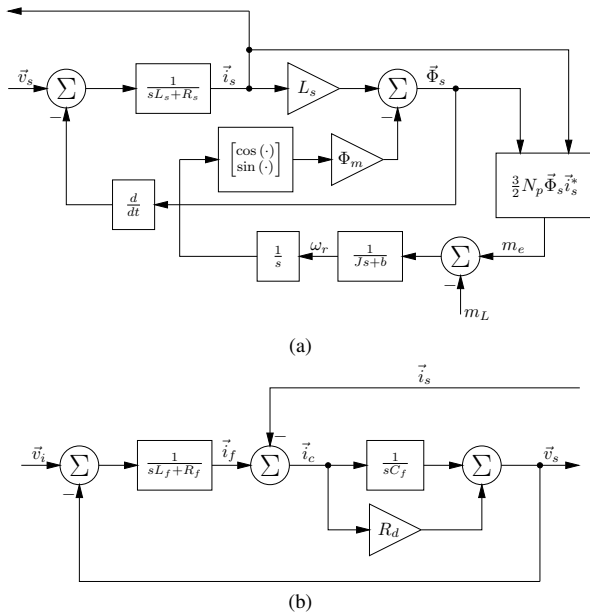


Fig. 7: The Simulink transfer function model for the filter-generator plant, with the RLC filter (a) and the PMSG (b).

The inverter and switching model, estimation blocks and control blocks are not shown here, due to space constraints. The Simulink simulation is implemented using only function blocks that are available with the basic distribution.

B. VHDL-AMS

The most important part of the simulation study is to implement the system in a VHDL-AMS simulation framework. Several simulation packages supporting VHDL-AMS have been tried and tested, and SystemVision from Mentor Graphics was found to be the most competent package.

Although SystemVision caters for graphical simulation design such as Simulink, the aim is to implement the simulation purely in VHDL-AMS to retain portability. This philosophy will allow the simulation to be easily ported to any other

⁴SystemVision does have graphical input capability, but it was the intention of the authors to use pure VHDL-AMS as the simulation method.

simulation package that supports VHDL-AMS. As the actual simulation code is too lengthy to be included in the paper in its entirety, only a diagram describing the simulation layout is provided. The diagram is shown in Fig. 8.

The structure of the VHDL-AMS simulation is what is referred to as a *testbench*, which is a ENTITY-ARCHITECTURE combination that provide a framework for the simulation. System-wide parameters are declared within the ENTITY declaration, to be used as constants in the simulation body.

The working of the simulation is declared within the ARCHITECTURE declaration. The variables are declared in the preamble of the ARCHITECTURE while the system models are described within the body.

The physical structure of the system is made up of lumped elements separated by nodes, including simultaneous equations that form part of the generator model. A PROCESS statement takes care of digital measurement, control and switch signal generation.

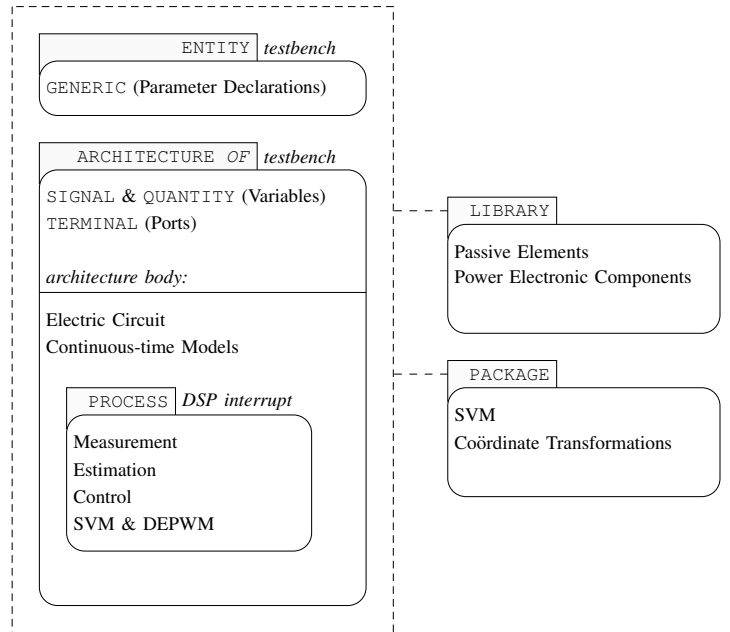


Fig. 8: Diagram representing the VHDL-AMS simulation.

A significant advantage of VHDL-AMS is the ease with which time-domain differential equations can be modelled. This modularity also allows for the simulation model to represent the physical system much more closely in structure. The digital difference equations can also be input exactly as they will be implemented in practice.

IX. SIMULATION RESULTS

Simulation results for torque steps of the DTC-SVM controlled system for VHDL-AMS and Simulink are given in Fig. 9. The starting electrical frequency for these torque steps is 50 Hz, which is a worst case scenario dynamically.

The system under variable speed operation is implemented in the VHDL-AMS simulation. A simple wind model is developed in [13] that models wind speed as the combination of base, ramp and gust wind speed. The ramp component is

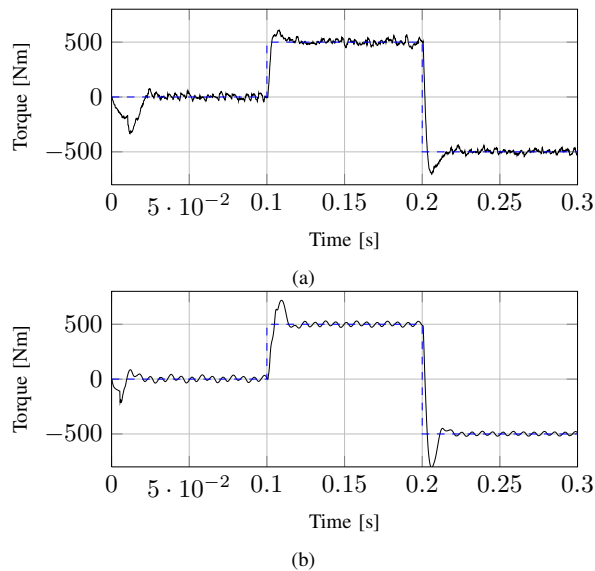


Fig. 9: Simulated torque steps for (a) VHDL-AMS in SystemVision and (b) MATLAB Simulink.

chosen to demonstrate the dynamic performance of the system in this simulation.

This simulation is not entirely a true reflection of reality, as the main input parameter should be the wind speed, with delivered turbine torque being a function of wind speed and rotor speed. It does however illustrate the dynamic performance of the system under ramp changes in turbine torque.

The results of this simulation over a 10 second interval is shown in Fig. 10. The dashed line represents the load torque delivered by the turbine. Observe how the system immediately changes as the variable speed algorithm is engaged very early in the simulation, after which convergence to the optimal working point commences.

X. PRACTICAL IMPLEMENTATION & RESULTS

The system is implemented practically on a laboratory test setup. The wind and wind turbine are represented by a torque controlled induction machine, controlled by a variable speed drive (VSD), that in turn drives the generator through a gearbox.

The PEC consists of a six switch IGBT bridge with an input RLC harmonic filter, controlled by a Texas Instruments eZDSP. A diagram depicting the laboratory setup is shown in Fig. 11.

State transitions of the system in full operation are shown in Fig. 13, where the dashed line represents the mechanical rotor speed and the solid line represents stator phase *a* current. It can be seen in Fig. 13(a) that the system transitions from the *Pre-cut-in* state to the *Cut-in* state at approximately 3s. The transition from *Cut-in* to *MPPT* is shown in Fig. 13(b), which is at about 4.7s. In Fig. 13(c) the transition takes place from *Max Speed* to *MPPT* just after 4s.

Care has to be taken in the transition states that the system does not get stuck in a limit cycle, as the system is inherently

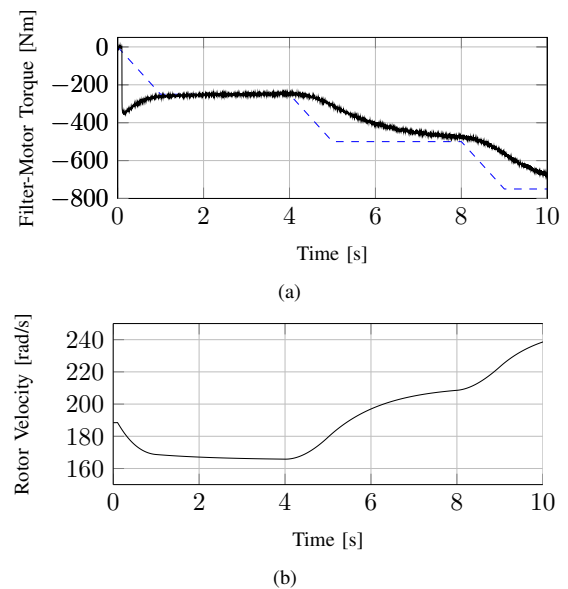


Fig. 10: Simulation results of variable speed operation of the system, showing (a) turbine torque & filter-generator torque and (b) electrical rotational speed of generator rotor.

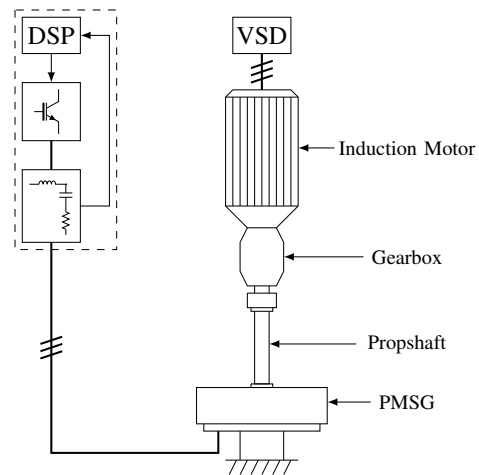


Fig. 11: Diagrammatic representation of the laboratory test setup.

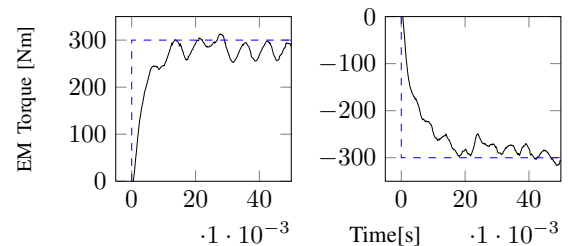


Fig. 12: Measured electromagnetic torque steps in both directions.

non-linear. If these regions are not traversed with care, the system may exhibit instabilities, which have been witnessed

TABLE III: Physical parameters of the WECS.

Parameter	Value
Rated line voltage	400 V
Rated current	35 A_{rms}
Rated rotational speed	150 rpm
Pole pairs (N_p)	20
Stator resistance (R_s)	0.4 Ω
Stator inductance (L_s)	10 mH
PM flux linkage (Φ_m)	1.0395 Wb-t
Rated torque	1000 Nm
Filter inductance (L_f)	600 μ H
Filter inductor resistance (r_f)	30 $m\Omega$
Filter capacitance (C_f)	47 μ F
Damping resistance (R_d)	10 Ω
Turbine moment of inertia (J)	300 $kg \cdot m^2$
Switching frequency (f_s)	10 kHz

in practical tests. The parameters of the transitions had to be tuned specifically to obtain best results.

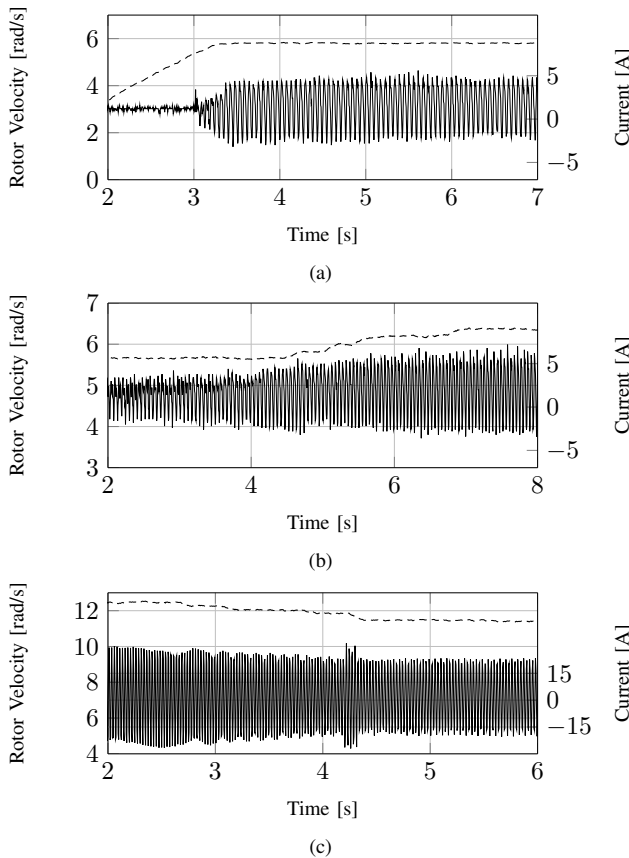


Fig. 13: Measured phase current and rotor speed of state transitions from (a) Pre-cut-in to Cut-in, (b) Cut-in to MPPT and (c) Max speed re-entry to MPPT.

XI. CONCLUSION

A complete mechanical sensorless, fixed pitch, variable speed WECS has been implemented on a DSP controlled

system. The system is modelled as a three-phase system, as well as in the $\alpha\beta$ - and xy -reference frames. Simulations are done in VHDL-AMS as well as MATLAB Simulink to verify the results. The system is implemented practically on a laboratory test setup.

The DTC controller gives good performance and correlates well with simulated data. The gain scheduling system, along with the speed control for state transitions and variable speed controller performs well.

Complete sensorless (small-scale) variable speed operation has been achieved by means of DTC-SVM of a PM wind generator through a RLC filter. Although the system has only been implemented in a laboratory test setup, the results indicate a high degree of probability that the system will perform well in practice.

The main contributions of this work include the expansion of the work done in [7] to address the dynamic effects of an RLC filter, and the application of the theory to a wind generation system. The modelling and simulation of the system in both VHDL-AMS and Simulink also present a significant contribution, as well as the verification of simulation results to those of Simulink.

REFERENCES

- [1] H. Li and Z. Chen, "Overview of different wind generator systems and their comparisons," *IET Renewable Power Generation*, vol. 2, no. 2, pp. 123–138, 2008.
- [2] J. Pontt, J. Rodriguez, M. Rotella, S. Kouro, C. Silva, and H. Farias, "Output sinus filter for medium voltage drive with direct torque control," in *Fourtieth IAS Annual Meeting. Conference Record of the 2005 Industry Applications Conference, 2005*. IEEE, pp. 204–209.
- [3] A. Sapin, P. Steimer, and J.-J. Simond, "Modeling, simulation and test of a three-level voltage source inverter with output LC filter and direct torque control," in *38th IAS Annual Meeting on Conference Record of the Industry Applications Conference, 2003*. IEEE, pp. 492–498.
- [4] Z. Xu, T. Pang, and X. Dianguo, "Instantaneous torque control of a permanent magnet wind power generator without a position sensor," *Electrical Machines and Systems, 2008. ICEMS 2008. International Conference on*, pp. 1343–1347.
- [5] C. Busca, A. Stan, T. Stanciu, and D. Stroe, "Control of Permanent Magnet Synchronous Generator for Large Wind Turbines," *Control*, no. 1.
- [6] J. M. Kwon, J. H. Kim, S. H. Kwak, and H. H. Lee, "Optimal power extraction algorithm for dtc in wind power generation systems," *2008 IEEE International Conference on Sustainable Energy Technologies*, no. 2, pp. 639–643, Nov. 2008.
- [7] D. Swierczynski, "Direct Torque Control with Space Vector Modulation (DTC-SVM) of Inverter-Fed Permanent Magnet Synchronous Motor Drive," Ph.D. dissertation, 2005.
- [8] I. K. Hobbs, "Evaluation and implementation of anti-islanding methods for converter-fed distributed generation," Stellenbosch, South Africa, 2009.
- [9] S. Mastellone, G. Papafotiou, and E. Liakos, "Model Predictive Direct Torque Control for MV drives with LC filters," *Power Electronics and Applications, 2009. EPE '09. 13th European Conference on*, pp. 1–10.
- [10] S. Yang, X. Zhang, C. Zhang, Z. Xie, and F. Li, "Sensorless control for PMSG in direct-drive wind turbines," in *The 2nd International Symposium on Power Electronics for Distributed Generation Systems*. IEEE, Jun. 2010, pp. 81–84.
- [11] M. P. Kazmierkowski, R. Krishnan, and F. Blaabjerg, *Control in Power Electronics*, 1st ed. Academic Press, 2002.
- [12] F. D. Bianchi, H. D. Battista, and R. J. Mantz, *Wind Turbine Control Systems: Principles, Modelling and Gain Scheduling Control*. Springer-Verlag London Limited, 2007.
- [13] A. Rolan, A. Luna, G. Vazquez, D. Aguilar, and G. Azevedo, "Modeling of a variable speed wind turbine with a Permanent Magnet Synchronous Generator," in *2009 IEEE International Symposium on Industrial Electronics*. IEEE, Jul. 2009, pp. 734–739.